Hindawi Publishing Corporation
Chinese Journal of Engineering
Volume 2016, Article ID 7124267, 9 pages
http://dx.doi.org/10.1155/2016/7124267

Research Article

Propagation Channel Comparison between 23.5 and 45 GHz in Conference Scenario

Jianwu Dou,[1] Nan Zhang,[1] Li Tian,[1] Xiaoyi Yang,[1] Xi Yuan,[1] Suping Mei,[1] and Haiming Wang[2]

[1] *Wireless Algorithm Department, Product R&D System, ZTE Corporation, Shanghai 201203, China*
[2] *State Key Laboratory of Millimeter Waves, Southeast University, No. 2, Sipailou, Nanjing 211111, China*

Correspondence should be addressed to Nan Zhang; zhang.nan152@zte.com.cn

Received 28 September 2015; Revised 26 January 2016; Accepted 9 February 2016

Academic Editor: Jungnickel Volker

The characteristics of propagation channel at 23.5 and 45 GHz in an indoor conference room are studied based on hybrid approach. A ray-based simulator which includes the reflection, penetration, diffraction, and diffuse scattering is adopted to generate the massive channel realizations. This platform is well calibrated in path and power delay profile (PDP) levels according to some specified measurements at different frequencies. Subsequently, according to the simulated channel samples, the statistical channel model for both the large and small scale characteristics is established based on the alpha-beta approach and extended Saleh-Valenzuela (S-V) structure, respectively. Results show that the slope of fitted path loss (PL) is less than free space due to the waveguide effect for both 23.5 and 45 GHz in indoor scenario and larger PL is experienced at higher frequency. Additionally, the cluster is more centralized with less spreads and decaying faster in delay domain at 45 GHz.

1. Introduction

For satisfying the increasing demands of the cellular system capacity and overcoming the spectrum congestion below 6 GHz, the millimeter wave is considered as a promising candidate for the fifth-generation (5G) communication systems [1–3]. Since the channel models have significant influences on the simulation for the performance evaluation of wireless communication techniques, the channel investigations at high frequency have been popular in both industry and academia.

In general, two mainstream methods, that is, measurement-based stochastic and ray-based deterministic approaches, are adopted to construct reliable channel models. Conventionally, the measurement-based approach dominates the channel investigation at low frequencies, namely, below 6 GHz. Many classical statistical channel models, such as WINNER II, 3GPP SCM, and ITU, are established in this way [4–6]. At high frequencies, due to the large propagation loss, the channel measurement campaigns, which were conducted by the platform equipped with horn antennas with large gain, are becoming popular [2, 7–9]. However, many drawbacks are also introduced; that is, the time consumption of the measurement is drastically increased; since that, the horn antennas need to be rotated for all azimuth-elevation pairs to capture the channel spatial characteristics at both Tx and Rx sides. And sufficient channel samples are difficult to be collected within the coherent time. Meanwhile, the resolution in spatial domain is limited by the rotation step of the antenna in measurement (usually equal to the half-power beamwidth (HPBW) of the horn antenna) and the radiation patterns are also slightly overlapped when the antennas are directed to different angles. It is difficult to eliminate the effects of antenna pattern when studying pure channel characteristics in both large and small scale. Therefore, the accuracy of the measurement-based model would not be persuasive as well.

Currently, researches show that the propagation channel in high frequency can be well reproduced by considering a few number of paths originating from different mechanism, that is, specular reflection, diffraction, and background scattering, due to the much more severe propagation and penetration loss [11, 12]. Thus, the ray-based deterministic modeling approaches with lower complexity have been found

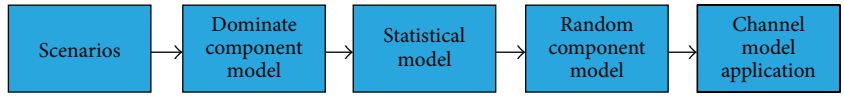

Figure 1: Diagram of the proposed hybrid modeling approach.

to be more suitable for studying the high-frequency channels since they are more flexible to be implemented in various cases under different configurations. Besides, the channel evolutionary behavior over time and spatial domains can be more accurately represented for new algorithm evaluation, that is, beam-tracking. However, the accuracy of ray-based model highly depends on the fineness of the digitized map and the calibration of the RT method is well done, that is, electromagnetic properties of the materials and the order of the interactions implemented in the simulation.

Considering the efficiency and accuracy of the channel modeling, a hybrid approach involving the intrinsic advantages of both measurement- and ray-based method is proposed in this paper. The diagram of procedures for this method is shown in Figure 1 and total 5 main steps are involved:

(1) The selected scenario refers to a specified case or a kind of scenes with well defined geometric and electromagnetic properties.

(2) The behaviors of the dominant components (dominant component refers to the specular rays with larger power, which are usually originating from direct LoS, reflection, and diffraction), that is, the distribution and time- or spatial-evolutionary characteristics, are well reproduced since they are directly calculated in the deterministic way.

(3) The statistical model stands for the features of propagation channel in cluster level. It can be obtained from massive channel samples which are taken from measurement or simulation based on a calibrated method. This part will be elaborated as in this paper.

(4) The random component represents the influence of human blockage (human blockage represents that one ray is blocked due to the existence of human and this effect can be studied in both larger scale and small scale level. In the large scale level, the human blockage can be modeled as additional shadow fading and, in small scale level, the influence on the propagation ray is studied [13–15]. Considering the application in high frequency, the second way is preferable) and blink rays (the blink ray refers to the ray originated from the randomly existing objects, i.e., the vehicle in outdoor cases and the ornaments in the indoor scenes, and these kinks of rays are mostly single bounce) in specified cases. These phenomenons are difficultly investigated by measurement due to the various configurations, and establishing statistical models based on the extensive simulation results is a preferable way.

(5) Finally, the obtained pure channel can be applied according to specified demand; that is, the channel can be combined with different antenna pattern, system configurations.

The rest of the paper is organized as follows. In Section 2, the data acquisition based on measurement and ray-tracing are introduced briefly. Section 3 elaborates the performance evaluation of the ray-tracing based on measurement data in different frequency. The modeling results and comparison are presented in Section 4. Finally, conclusive remarks are given in Section 5.

2. Data Acquisition

2.1. Measurement Campaign. The channel measurement is conducted in a typical indoor conference room located in the wireless valley, Nanjing, China. The panorama of the environment is depicted in Figure 2. Measurements have been carried out in a static configuration; that is, the transmitter (Tx) was located in a high corner of room to emulate an access point, and the receiver (Rx) as shown in Figure 2 has been moved in 10 and 30 different locations at 45 and 23.5 GHz, respectively.

For each position, the channel frequency response has been recorded by using the automatic channel sounding system [16]. An Agilent signal generator E8257D was used in Tx site and an Agilent VNA N5245A in frequency-sweep mode was adopted to collect the channel frequency response in Rx site. Both of them are synchronized by the common reference signal source. The measurement procedure and data storage were controlled by a computer. Two vertical-polarized horn antennas were installed on the customer-made rotary tables at both the Tx and Rx terminals. At each Rx position, the spatial channel information is captured by rotating the Tx and Rx in both azimuth and elevation domains successively. The measurement configurations are listed in Table 1 and more details about the measurement campaign can be found in [16]. The peak detection method is used to identify the path in delay domain, and the spatial parameters are assigned according to the boresights of rotated antenna pairs with the spatial resolution limited by the rotating step.

2.2. Ray-Tracing Simulation. A self-developed ray-tracing (RT) software was implemented in this research. Total three main steps are involved to generate the channel realizations, that is, constructing the 3D digital map for specified scenario, calculating the geometric trace for each ray, and adopting the electromagnetic properties according to simulation configurations. The digitized map is built by measuring the geometric parameters of all the major objects (such as

Figure 2: Panorama of the indoor measurement environment.

Table 1: Channel sounding configurations.

Parameter	Settings	
Center frequency	44.955 GHz	23.5 GHz
Bandwidth	660 MHz	
Transmit power	10 dBm	
Antenna type	Linearly polarized horn antenna	
Antenna gain	23.7 dBi	18.9 dBi
Half-power beamwidth	11°	18.2°
Sweep frequency points	256	
Sweep frequency duration	80 ms	
Cycles per measurement	8	
Tx height	1.95 m	
Rx height	1 m	

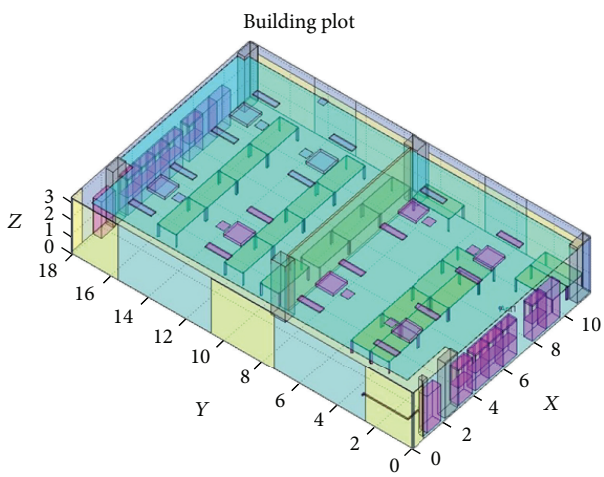

Figure 3: Digitized map for the specified scenario.

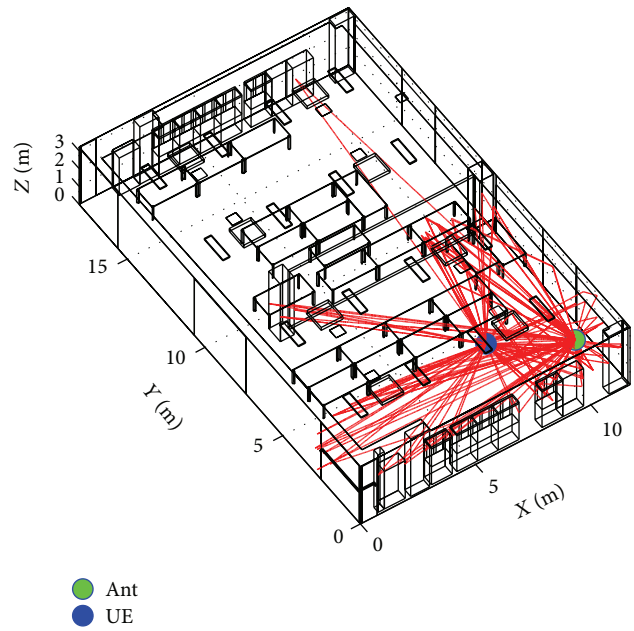

Figure 4: Illustration of the specular paths simulated by ray-tracing for the specified scenario.

walls, tables, bookshelves, coated glasses, etc.) in the room. Then, a commercial software "Sketchup Pro" [17] is used to reconstruct the scenario as shown in Figure 3.

The propagation paths which originate from the propagation mechanisms of line-of-sight (LoS), reflection, diffraction, and penetration, are identified by the aforementioned 3D image-based RT platform. The complex coefficients of LoS and reflected and diffracted ray are calculated according to the free-space Friis equation, Fresnel formulas, and the uniform theory of diffraction (UTD) [18–20], respectively. Meanwhile, at high frequencies, the nonnegligible diffuse scattering, which refers to the back-reflection from rough surfaces or nonhomogenous materials, is implemented by adopting the directive scattering pattern based on the "effective roughness" (ER) scattering model [21–24]. The rough surfaces of each object are discretized into multiple small tiles, and for each tile the far-field assumption should be satisfied. Under noncoherent assumption, the phase of each scattering path is randomly assigned.

The digitalized map of this scene is shown in Figure 3 with the color-coded materials. The calibrated electromagnetic properties (i.e., relative permittivity and conductivity) at specified frequency are adopted [25]. At most, 3 reflections, 1 diffraction, and 1 scattering together with 10 penetrations are considered in our simulation by considering the trade-off between modeling accuracy and complexity. An example of the simulated specular paths by using ray-tracing tool is illustrated in Figure 4. The other configurations such as bandwidth, transmit power, and antenna radiation patterns are the same as the measurement for further RT calibration.

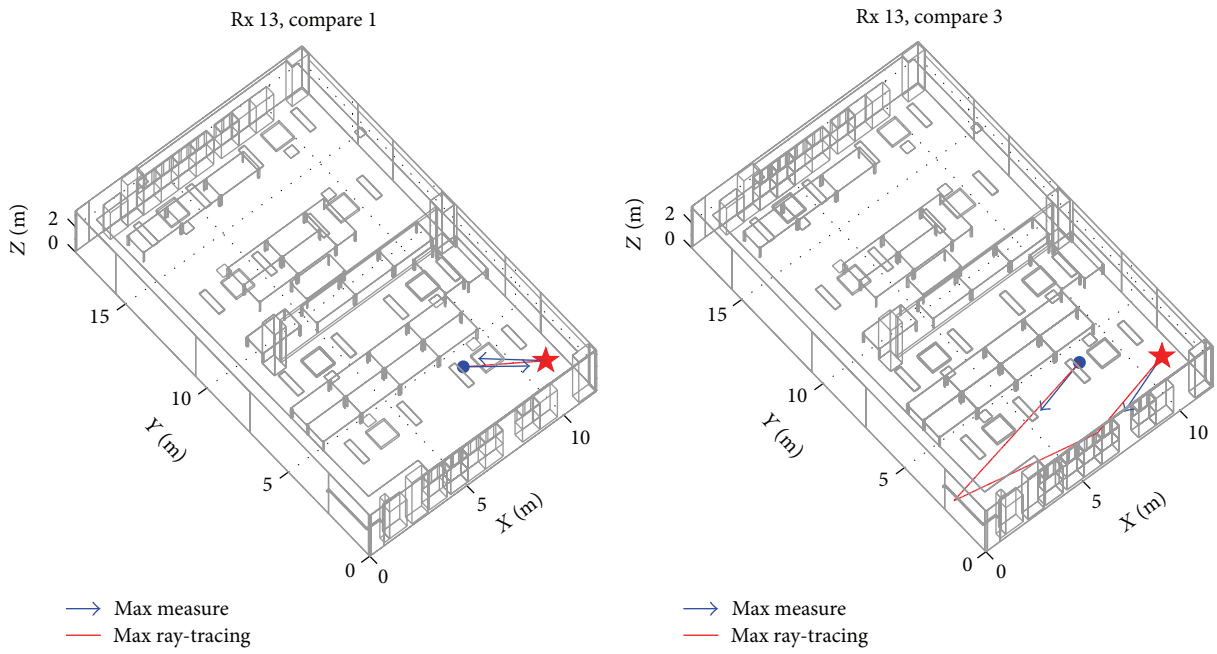

(a) LoS path (b) Two-bounce reflection

Figure 5: An example of ray-level comparison between measurement and simulation.

3. Performance Evaluation of the RT Simulator

Before conducting the extensive simulations to generate the channel realizations, the RT software is calibrated in two aspects with different measurement configurations. According to the proposed hybrid channel model approach shown in Figure 1, the framework of the propagation channel is determined by the dominant components, so the specular path level comparison between the measurement and simulation is done firstly.

Figure 5 illustrates the ray comparison between measurement and simulation. The blue lines with arrow refer to the direction of the ray obtained from the measurement, and the red solid lines illustrate the trace for the same path based on RT simulator. It can be found that the dominant paths, that is, LoS and double bounces reflection paths, are well matched. The slight mismatches in the direction are observed since the spatial resolution of the measurement is limited by the antenna rotation step. This phenomenon also demonstrates that the performance of current measurement-based channel modeling approach is easily affected by the measurement configurations.

The power-delay-profile (PDP) which depicts the power decaying phenomena along the travel distance is used as a common metric for the evaluation of multipath channel simulation. The measurement-based PDP is derived from the captured channel frequency response as

$$P(\tau) = |h(\tau)|^2, \qquad h(\tau) = \mathcal{F}^{-1}[H(f)], \tag{1}$$

where $H(f)$ is the channel transfer function in the frequency domain, $h(\tau)$ means the channel impulse response (CIR) in the delay domain, and $\mathcal{F}^{-1}$ denotes the inverse Fourier transfer. Simulation results are obtained from the RT software with the calibrated parameters, that is, directivity $\alpha = 1$ and $\alpha = 10$ for 23.5 GHz and 45 GHz, respectively, with the same scattering coefficient $S = 0.8$, in ER model. The verifications for these parameters in diffuse scattering are conducted by calculating the minimum mean square error (MMSE) between the measured and simulated PDP. The parameter values which lead to the smallest MMSE are adopted as in [11, 22, 26].

The comparison of the PDPs is shown in Figure 6, where the the measured PDP, simulation results of specular RT (the specular RT refers to the RT only involving the LoS, penetration, reflection, and diffraction, no diffuse scattering effect is considered), and the combination of the specular RT and scattering are demonstrated. It can be observed from the comparison results that (1) most of the dominant components are captured by ray-tracing simulation, (2) the specular peaks in the PDP are extended to cluster-alike dispersive components and more realistic and continuous PDPs are obtained by adopting scattering phenomenon in RT method. and (3) some strong components around 100 ns and 70 ns can also be found in the PDP of 23.5 and 45 GHz, respectively. By comparing the room size with the large travel distance for these paths, we speculate that wave reverberation is also significant in such kind of indoor room. Therefore, multiple bounces paths, that is, diffuse scattering or specular reflection combined with scattering [22, 27], should be implemented in RT if the time consumption for simulation is acceptable.

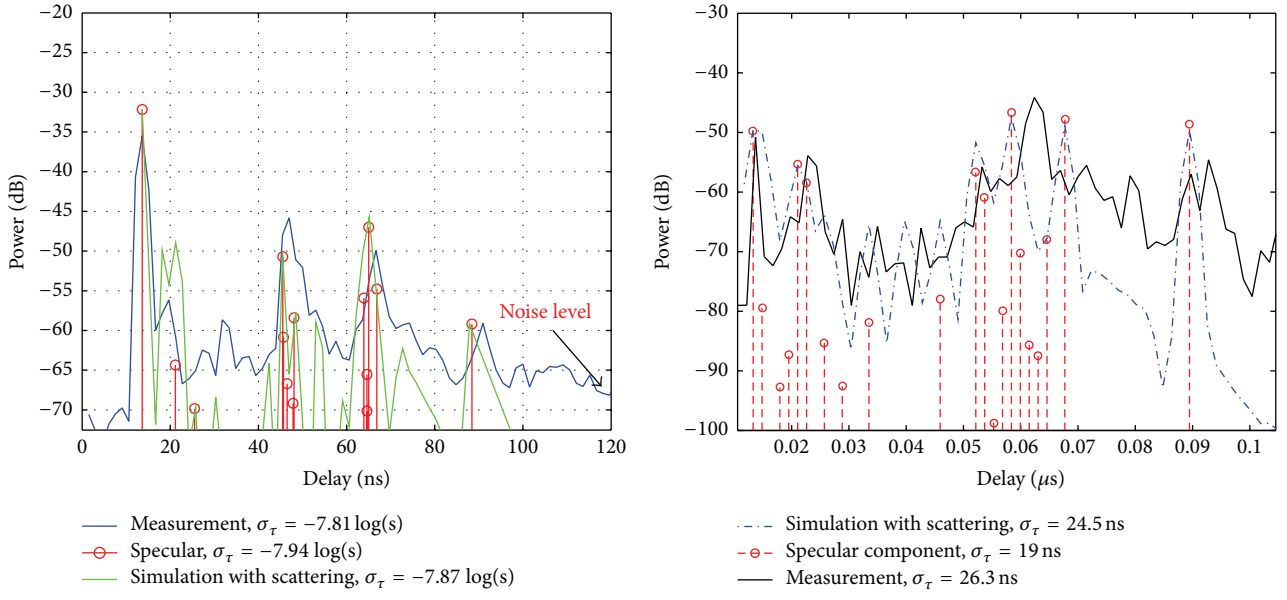

(a) PDP comparison at 23.5 GHz

(b) PDP comparison at 45 GHz [10]

Figure 6: Comparison of the power delay profiles.

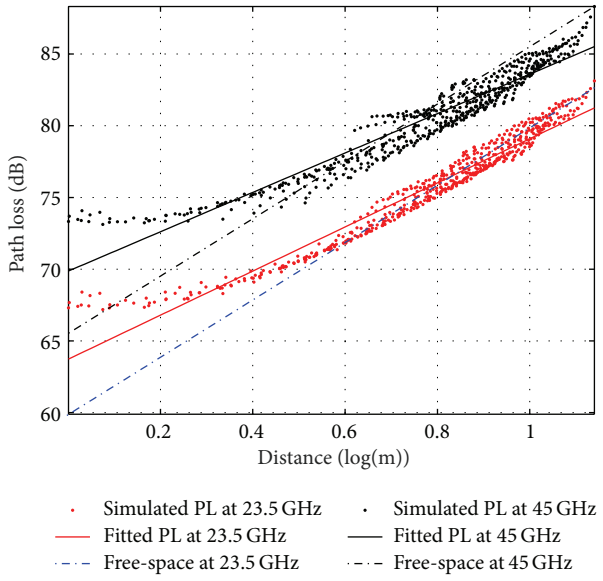

Figure 7: Path loss comparison in LoS scenario.

4. Modeling Results

After the validation of the RT tool, it is further adopted to generate massive channel samples. In the extensive simulations, ideal isotropic antennas are used in both Tx and Rx sides. The Tx is stable at the location as shown in Figure 4 and the Rx is assumed to move within the whole room with a step of 0.2 m. Totally, 4500 snapshots of channel data are collected and the statistical channel model for both large and small scale parameters are established based on these samples.

Table 2: Path loss and shadow fading.

Parameters	23.5 GHz		45 GHz	
	LoS	NLoS	LoS	NLoS
Path loss	(15.38, 63.72)	(17.81, 70.45)	(13.73, 69.86)	(18, 74.46)
σ_{SF}	0.89	1.53	0.97	1.57

4.1. Larger Scale Channel Model. The path loss (PL) for both frequencies and scenarios is described by the alpha-beta model as [28]

$$\mathrm{PL}(d) = \alpha \cdot \log(d) + \beta + \sigma_{\mathrm{SF}}, \quad (2)$$

where d means the distance between Tx and Rx. α and β are the slope and intercept for the fitted path loss, respectively. σ_{SF} stands for the standard deviation of the shadow fading (SF) following the log-normal distribution with the mean equal to zero.

The comparisons of PL in LoS and NLoS at different frequency are depicted by Figures 7 and 8, respectively. Comparing with the 23.5 GHz, larger PLs can be found at 45 GHz in both LoS and NLoS cases. Due to the waveguide-like effect in indoor environment, the slopes of all fitted PL are less than free space [29, 30]. Since the distributions of the samples are dispersive in both 23.5 and 45 GHz, severer SFs are also observed in NLoS scenarios and the detail of fitted parameters are listed in Table 2.

4.2. Small Scale Channel Model. For good understanding of the channel characteristics, the signal model of the channel

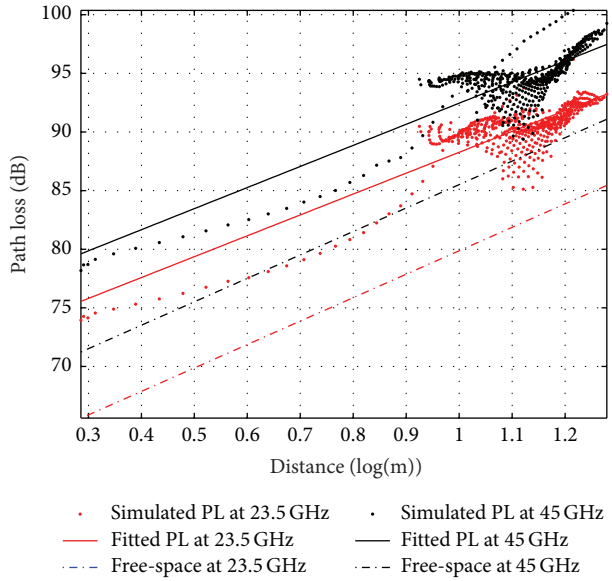

Figure 8: Path loss comparison in NLoS scenario.

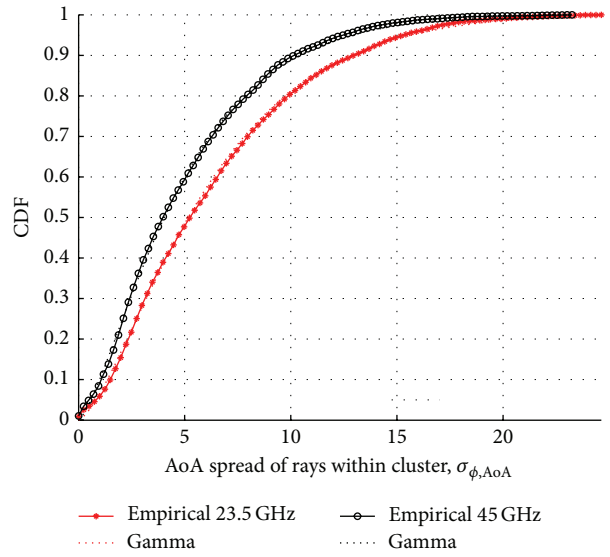

Figure 9: CDF comparison AoA spread of rays within cluster in LoS.

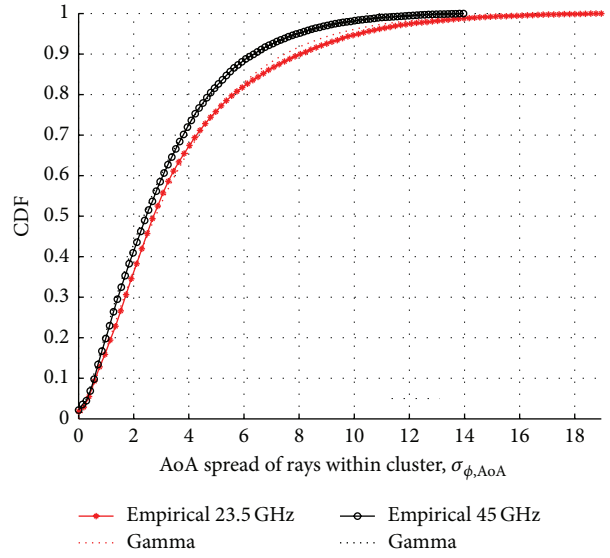

Figure 10: CDF comparison AoA spread of rays within cluster in NLoS.

impulse response (CIR) is implemented to analyze the small scale parameters as

$$h(t,\boldsymbol{\Theta}) = \sum_{l=1}^{L}\sum_{k=1}^{K}\alpha^{(l,k)}\cdot\delta\left(t-\tau^{(l,k)}\right)\cdot\delta\left(\phi_{\mathrm{Tx}}-\phi_{\mathrm{Tx}}^{(l,k)}\right) \cdot\delta\left(\theta_{\mathrm{Tx}}-\theta_{\mathrm{Tx}}^{(l,k)}\right)\cdot\delta\left(\phi_{\mathrm{Rx}}-\phi_{\mathrm{Rx}}^{(l,k)}\right)\cdot\delta\left(\theta_{\mathrm{Rx}}-\theta_{\mathrm{Rx}}^{(l,k)}\right), \tag{3}$$

where $\boldsymbol{\Theta} = [\alpha, \tau, \phi_{\mathrm{Tx}}, \theta_{\mathrm{Tx}}, \phi_{\mathrm{Rx}}, \theta_{\mathrm{Rx}}]$ represents the parameter set consisting of complex channel coefficient, azimuth of departure (AoD), elevation of departure (EoD), azimuth of arrival (AoA), and elevation of arrival (EoA), respectively. (l, k) refers to the kth path in the ith cluster.

The clustering results of the simulated channel realizations, which are obtained based on K-power mean algorithm, are used to establish the statistical channel model under extended S-V framework [31, 32]. The distributions of the inter- and intracluster parameters, that is, cluster arrival rate (Λ), cluster decay factor (Γ), cluster log-normal standard deviation σ_1, power of first ray, ray arrival rate λ, ray decay factor (γ), directional spreads (AoA, EoA, AoD, and EoD), and ray log-normal σ_2, are investigated empirically and these best fitted distributions for all parameters are selected based on Kolmogoroff-Smirnoff (K-S) test.

Figures 9 and 10 depict the comparison of the cluster AoA spread for both 23.5 and 45 GHz in LoS and NLoS scenarios, respectively. The Gamma distribution with different parameters is adopted to fit these results. Comparing with the results at 23.5 GHz, smaller cluster AoA spread is observed at 45 GHz and the same trends are found for other angular spreads. It means that the cluster is more concentrated in spatial domain at high frequency. Meanwhile, the spreads in elevation domain is less, but not significant, than the results in azimuth domain, which means that the channel diversity in the elevation domain is nonneglectable, especially in the indoor scenarios with small geometric size. From the simulation results, we also find that the cluster angular spreads in NLoS case are smaller comparing with LoS case. This is strange but reasonable by further investigating the environment settings in our simulation. As shown in Figure 5, the Tx locates at half part of the conference and the the whole room is naturally separated as LoS and NLoS by the wall in the middle. For the UE in the NLoS, the propagation rays mainly originate from the penetration through the wall and reflection from the coated glass as shown in Figure 3. Due to the larger propagation, penetration loss, and limited reflections, the incident angular range and power of the received rays are less than the UE in LoS, and it leads to smaller angular spreads.

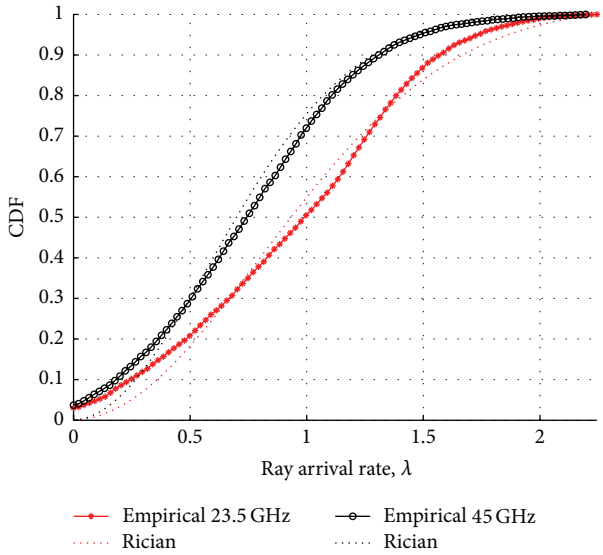

Figure 11: CDF comparison ray arrival rate in LoS.

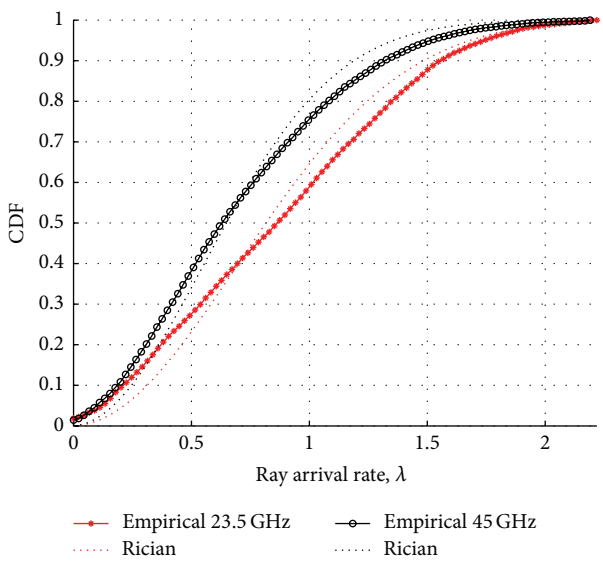

Figure 12: CDF comparison ray arrival rate in NLoS.

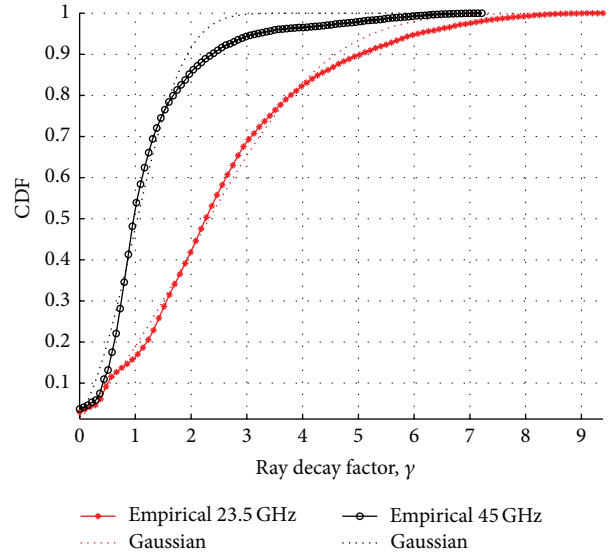

Figure 13: CDF comparison ray decay factor in LoS.

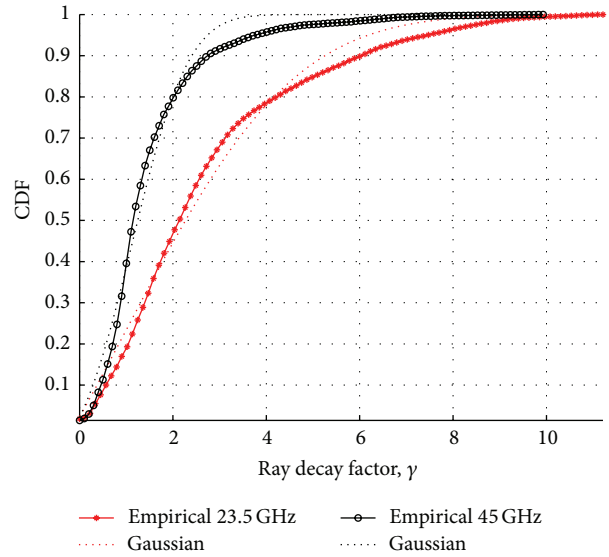

Figure 14: CDF comparison ray decay factor in NLoS.

The same comparisons for the ray arrival rate within the cluster are demonstrated in Figures 11 and 12. The obtained results are fitted by the Rician distribution and smaller λ is found at 45 GHz for both LoS and NLoS cases. Figures 13 and 14 illustrate the general trends of the ray decay factor in different cases and the Gaussian distribution is used to model the simulated results. From these figures, we can find that the rays within cluster decay faster at 45 GHz with regard to the 23.5 GHz. The aforementioned comparison results for λ and γ show that the cluster at 45 GHz is more concentrated than 23.5 GHz. More details about the statistical model can be found in Table 3.

5. Conclusions

In this contribution, a hybrid channel modeling approach, which involves the advantages of both deterministic simulation and measurement-based statistical analysis, was proposed. The calibrations of the RT simulator were firstly done in path and PDP levels through the comparison among simulation and measurement results. And the calibration results showed that the effect of diffuse scattering is also important at high frequencies. Subsequently, the statistical model for large and small scale channel parameters was established according to the obtained massive simulated channel realizations. It has been found that the PL is larger and the cluster is more concentrated at 45 GHz.

Table 3: Statistical channel model for 45 and 23.5 GHz based on S-V structure.

Parameters	Fitted distribution	23.5 GHz		45 GHz	
		LoS	NLoS	LoS	NLoS
Power of first ray	Gamma	(0.05, 5.00)	(0.07, 3.40)	(0.04, 8.90)	(0.01, 2.20)
Cluster arrival rate Λ [ns]	Uniform	(7.32, 33.47)	(15.00, 46, 18)	(6.97, 31.54)	(13.18, 44.54)
Cluster decay factor Γ [ns]	Gaussian	(2.28, 2.17)	(5.30, 2.79)	(3.78, 1.60)	(4.32, 2.15)
Cluster lognormal std σ_1 [dB]		1.65	2.15	2.17	2.79
Ray arrival rate λ [ns]	Rician	(0.13, 0.81)	(0.09, 0.70)	(0.15, 0.59)	(0.15, 0.55)
Ray decay factor γ [ns]	Gaussian	(2.05, 1.90)	(1.09, 2.80)	(1.01, 0.73)	(1.18, 0.95)
Cluster AoA spread (deg)	Gamma	(3.85, 1.70)	(2.43, 1.50)	(3.24, 1.60)	(2.24, 1.40)
Cluster EoA spread (deg)	Gamma	(3.65, 1.40)	(3.19, 1.00)	(2.04, 2.00)	(2.19, 1.00)
Cluster AoD spread (deg)	Gamma	(5.11, 1.40)	(2.58, 1.60)	(3.51, 1.50)	(2.00, 1.70)
Cluster EoD spread (deg)	Gamma	(4.62, 1.30)	(3.49, 1.10)	(3.19, 1.40)	(2.40, 1.30)
Ray lognormal std σ_2 [dB]		0.45	0.52	0.45	0.46

Conflict of Interests

The authors declare that there is no conflict of interests regarding the publication of this paper.

Acknowledgment

This work is supported by the project "Next-Generation Wireless Broadband Mobile Communications Networks" (no. 2014ZX03003012).

References

[1] METIS, "Deliverable d1.1 scenarios, requirements and KPIs for 5G mobile and wireless system," Tech. Rep. ICT-317669-METIS/D1.1, Mobile and Wireless Communications Enablers for the Twenty-Twenty Information Society (METIS), 2014.

[2] T. Rappaport, S. Sun, R. Mayzus et al., "Millimeter wave mobile communications for 5G cellular: it will work!," *IEEE Access*, vol. 1, pp. 335–349, 2013.

[3] A. Ghosh, T. A. Thomas, M. C. Cudak et al., "Millimeter-wave enhanced local area systems: a high-data-rate approach for future wireless networks," *IEEE Journal on Selected Areas in Communications*, vol. 32, no. 6, pp. 1152–1163, 2014.

[4] J. Meinila, "Winner+ final channel models," Tech. Rep., Wireless World Initiative New Radio, lC WINNER+, 2010.

[5] 3GPP, "Study on 3D channel model for LTE," Tech. Rep. 3GPP TR 36.873 V1.2.0 (2013-09), R1-136084, 2013, (release 12).

[6] ITU, "Guidelines for evaluation of radio interface technologies for imtadvanced," Tech. Rep. ITU-R M.1645, 2008.

[7] J. N. Murdock, E. Ben-Dor, Y. Qiao, J. I. Tamir, and T. S. Rappaport, "A 38 GHz cellular outage study for an urban outdoor campus environment," in *Proceedings of the IEEE Wireless Communications and Networking Conference (WCNC '12)*, pp. 3085–3090, Shanghai, China, April 2012.

[8] S. Hur, Y.-J. Cho, J. Lee, N.-G. Kang, J. Park, and H. Benn, "Synchronous channel sounder using horn antenna and indoor measurements on 28 GHz," in *Proceedings of the IEEE International Black Sea Conference on Communications and Networking (BlackSeaCom '14)*, pp. 83–87, IEEE, Odessa, Ukraine, May 2014.

[9] S. Hur, Y.-J. Cho, T. Kim et al., "Wideband spatial channel model in an urban cellular environments at 28 GHz," in *Proceedings of the 9th European Conference on Antennas and Propagation (EuCAP '15)*, pp. 1–5, Lisbon, Portugal, April 2015.

[10] J. Dou, L. Tian, H. Wang, X. Yuan, N. Zhang, and S. Mei, "45GHz propagation channel modeling for an indoor conference scenario," in *Proceedings of the 26th Annual International Symposium on Personal, Indoor, and Mobile Radio Communications (PIMRC '15)*, pp. 2225–2228, IEEE, Hong Kong, China, August 2015.

[11] V. Degli-Esposti, F. Fuschini, E. M. Vitucci et al., "Ray-tracing-based mm-wave beamforming assessment," *IEEE Access*, vol. 2, pp. 1314–1325, 2014.

[12] F. Fuschini, E. M. Vitucci, M. Barbiroli, G. Falciasecca, and V. Degli-Esposti, "Ray tracing propagation modeling for future small-cell and indoor applications: a review of current techniques," *Radio Science*, vol. 50, no. 6, pp. 469–485, 2015.

[13] M. Jacob, S. Priebe, T. Kurner et al., "Fundamental analyses of 60 GHz human blockage," in *Proceedings of the 7th European Conference on Antennas and Propagation (EuCAP '13)*, pp. 117–121, Gothenburg, Sweden, April 2013.

[14] M. Jacob, S. Priebe, A. Maltsev, A. Lomayev, V. Erceg, and T. Kurner, "A ray tracing based stochastic human blockage model for the IEEE 802.11ad 60 GHz channel model," in *Proceedings of the the 5th European Conference on Antennas and Propagation (EUCAP '11)*, pp. 3084–3088, IEEE, April 2011.

[15] D. Cassioli and N. Rendevski, "A statistical model for the shadowing induced by human bodies in the proximity of a mmWaves radio link," in *Proceedings of the IEEE International Conference on Communications Workshops (ICC '14)*, pp. 14–19, IEEE, Sydney, Australia, June 2014.

[16] J. Zhu, H. Wang, and W. Hong, "Large-scale fading characteristics of indoor channel at 45-ghz band," *IEEE Antennas and Wireless Propagation Letters*, vol. 14, pp. 735–738, 2015.

[17] A. Chopra, *Introduction to Google Sketchup*, John Wiley & Sons, 2012.

[18] H. Friis, "A note on a simple transmission formula," *Proceedings of the IRE*, vol. 34, no. 5, pp. 254–256, 1946.

[19] R. M. Azzam and N. M. Bashara, *Ellipsometry and Polarized Light*, North-Holland, Elsevier Science, 1987.

[20] R. G. Kouyoumjian and P. H. Pathak, "A uniform geometrical theory of diffraction for an edge in a perfectly conducting surface," *Proceedings of the IEEE*, vol. 62, no. 11, pp. 1448–1461, 1974.

[21] J. Järveläinen and K. Haneda, "Sixty gigahertz indoor radio wave propagation prediction method based on full scattering model," *Radio Science*, vol. 49, no. 4, pp. 293–305, 2014.

[22] L. Tian, V. Degli-Esposti, E. M. Vitucci, X. Yin, F. Mani, and S. X. Lu, "Semi-deterministic modeling of diffuse scattering component based on propagation graph theory," in *Proceedings of the 25th Annual International Symposium on Personal, Indoor, and Mobile Radio Communication (PIMRC '14)*, pp. 155–160, IEEE, Washington, DC, USA, September 2014.

[23] C. Jansen, S. Priebe, C. Moller et al., "Diffuse scattering from rough surfaces in THz communication channels," *IEEE Transactions on Terahertz Science and Technology*, vol. 1, no. 2, pp. 462–472, 2011.

[24] V. Degli-Esposti, F. Fuschini, E. M. Vitucci, and G. Falciasecca, "Measurement and modelling of scattering from buildings," *IEEE Transactions on Antennas and Propagation*, vol. 55, no. 1, pp. 143–153, 2007.

[25] ITU, "Effects of building materials and structures on radiowave propagation above about 100 mhz," Recommendation ITU-R P 2040-1, 2015.

[26] E. M. Vitucci, F. Mani, V. Degli-Esposti, and C. Oestges, "Polarimetric properties of diffuse scattering from building walls: experimental parameterization of a ray-tracing model," *IEEE Transactions on Antennas and Propagation*, vol. 60, no. 6, pp. 2961–2969, 2012.

[27] T. Pedersen, G. Steinbock, and B. H. Fleury, "Modeling of reverberant radio channels using propagation graphs," *IEEE Transactions on Antennas and Propagation*, vol. 60, no. 12, pp. 5978–5988, 2012.

[28] G. R. Maccartney, J. Zhang, S. Nie, and T. S. Rappaport, "Path loss models for 5G millimeter wave propagation channels in urban microcells," in *Proceedings of the IEEE Global Communications Conference (GLOBECOM '13)*, pp. 3948–3953, IEEE, Atlanta, Ga, USA, December 2013.

[29] METIS, "Deliverable d1.4 metis channel model," Tech. Rep. ICT-317669-METIS/D1.4, Mobile and Wireless Communications Enablers for the Twenty-Twenty Information Society (METIS), 2015.

[30] G. Kalivas, M. El-Tanany, and S. Mahmoud, "Millimeter-wave channel measurements for indoor wireless communications," *IEEE Transactions on Vehicular Technology*, vol. 44, no. 3, pp. 494–505, 2002.

[31] A. Saleh and R. Valenzuela, "A statistical model for indoor multipath propagation," *IEEE Journal on Selected Areas in Communications*, vol. 5, no. 2, pp. 128–137, 1987.

[32] S. Kato, H. Harada, R. Funada et al., "Single carrier transmission for multi-gigabit 60-GHz WPAN systems," *IEEE Journal on Selected Areas in Communications*, vol. 27, no. 8, pp. 1466–1478, 2009.